Author Manuscript

Author Manuscript

Author Manuscript

Author Manuscript

HHS Public Access

Author manuscript

Mol Imaging Biol. Author manuscript; available in PMC 2021 November 25.

Published in final edited form as:

Mol Imaging Biol. 2020 October ; 22(5): 1427–1437. doi:10.1007/s11307-019-01455-x.

Near-Infrared Imaging with Second-Window Indocyanine Green in Newly Diagnosed High-Grade Gliomas Predicts Gadolinium Enhancement on Postoperative Magnetic Resonance Imaging

Steve S. Cho, BS[1,2], **Ryan Salinas, MD**[2], **Emma De Ravin, BS**[1,2], **Clare W. Teng, BS**[1,2], **Carrie Li, BS**[1,2], **Kalil G. Abdullah, MD**[2], **Love Buch, BS**[2], **Jasmin Hussain, BS**[2], **Fahad Ahmed**[2], **Jay Dorsey, MD, PhD**[3], **Suyash Mohan, MD**[4], **Steven Brem, MD**[2], **Sunil Singhal, MD**[5], **John Y.K. Lee, MD, MSCE**[2]

[1]Perelman School of Medicine at the University of Pennsylvania, Philadelphia, PA

[2]Department of Neurosurgery at the Hospital of the University of Philadelphia, Philadelphia, PA

[3]Department of Radiation Oncology at the Hospital of the University of Philadelphia, Philadelphia, PA

[4]Department of Radiology at the Hospital of the University of Philadelphia, Philadelphia, PA

[5]Department of Surgery at the Hospital of the University of Philadelphia, Philadelphia, PA

Abstract

Purpose: Intraoperative molecular imaging with tumor-targeting fluorophores offers real-time detection of neoplastic tissue. The Second-Window-Indocyanine-Green (SWIG) technique relies on passive accumulation of indocyanine-green (ICG), a near-infrared fluorophore, in neoplastic tissues.In this study, we explore the ability of SWIG to detect neoplastic tissue and to predict postoperative Magnetic Resonance Imaging (MRI) findings intraoperatively.

Procedures: Retrospective data were collected from 36 patients with primary high-grade gliomas (HGG) enrolled as part of a larger trial between October 2014 and October 2018. Patients received systemic ICG infusions at 2.5–5mg/kg 24 h preoperatively. Near-infrared fluorescence was recorded throughout the case and from biopsy specimens. The presence/location of residual SWIG signal after resection was compared to the presence/location of residual gadolinium enhancement on postoperative MRI. The extent of resection was not changed based on near-infrared imaging.

Terms of use and reuse: academic research for non-commercial purposes, see here for full terms. http://www.springer.com/gb/open-access/authors-rights/aam-terms-v1

Corresponding author: John Y.K. Lee, MD, MSCE., Address: 235 South Eight Street, Philadelphia, PA 19106, Phone: 215-829-6700, Fax: 215-829-6645, leejohn@uphs.upenn.edu.

Conflict of interest

None

Publisher's Disclaimer: This Author Accepted Manuscript is a PDF file of a an unedited peer-reviewed manuscript that has been accepted for publication but has not been copyedited or corrected. The official version of record that is published in the journal is kept up to date and so may therefore differ from this version.

Author Manuscript Author Manuscript Author Manuscript Author Manuscript

Results: All 36 lesions demonstrated strong near-infrared fluorescence (signal-to-background = 6.8 ± 2.2) and 100% of tumors reaching the cortex were visualized before durotomy. In 78 biopsy specimens, near-infrared imaging demonstrated higher sensitivity and accuracy than white-light for diagnosing neoplastic tissue intraoperatively. Furthermore, near-infrared imaging predicted gadolinium enhancement on postoperative MRI with 91% accuracy, with visualization of residual enhancement as small as $0.3cm^3$. Patients with no residual near-infrared signal after resection were significantly more likely to have complete resection on postoperative MRI (p-value < 0.0001).

Conclusions: Intraoperative imaging with SWIG demonstrates highly sensitive detection of HGG tissue in real-time. Furthermore, post-resection near-infrared imaging correlates with postoperative MRI. Overall, our findings suggest that SWIG can provide surgeons with MRI-like results in real-time, potentially increasing resection rates.

Keywords

Indocyanine-green; Near-infrared imaging; High-grade gliomas; Intraoperative MRI; Postoperative MRI

Introduction

Cancer remains a leading cause of death in the US. While the medical community continues to develop novel medical treatments, surgical resection still plays a major role in the diagnosis, treatment, and palliation of most solid cancers and this remains true in the treatment and palliation of high-grade gliomas (HGG). Numerous retrospective studies have demonstrated that increasing the extent of resection of gadolinium-enhancing components is independently associated with improved patient outcomes in patients with HGGs [1–5]. To achieve maximal safe resection, neurosurgeons often rely on extra tools in the operating room, such as neuronavigation, intraoperative magnetic resonance imaging (iMRI), intraoperative rapid pathology, and/or intraoperative ultrasound [6–10]. Neuronavigation, now widely adopted, relies on preoperative MRI sequences, which do not provide real-time, updated evaluation of the tumor margin intraoperatively. Conversely, iMRI can provide nearly real-time evaluation of the tumor margin and its use has been associated with increased extent of resection in HGG surgery [11]. However, the benefits of iMRI over conventional neuronavigation in improving HGG patient outcomes is unclear, with most studies favoring iMRI in increasing the extent of resection but without significant effects on overall survival [12–15]. Considering that iMRI is costly and time-consuming, the lack of strong evidence for its benefit currently limits its utility in many hospitals [11–13, 16, 17].

In contrast to the expensive and cumbersome iMRI, fluorescence-guided surgery (FGS) has recently emerged as a rapid and cost-effective method for intraoperative tumor visualization. Specifically, the administration of 5-aminolevulinic-acid (5-ALA) leads to the accumulation of a visible fluorophore protoporphyrin-IX in neoplastic cells [18]. FGS with 5-ALA, FDA-approved in 2017, has demonstrated increased resection rates and improved progression-free survival [19]. However, there is an increasing trend in favor of near-infrared (NIR) fluorophores over visible-spectrum fluorophores [20, 21] because NIR visualization offers improved tumor visualization due to superior photon penetration (>1cm

Author Manuscript Author Manuscript Author Manuscript Author Manuscript

vs <1mm) and minimal background auto-fluorescence leading to stronger contrast [22–24]. Furthermore, NIR fluorescence can easily be overlaid over white-light imaging due to the non-overlapping excitation/emission characteristics, allowing the surgeon to appreciate areas of NIR fluorescence in the context of background information. Given this trend, our group has investigated the benefits of a novel technique, Second-Window-Indocyanine-Green (SWIG). When given in high doses, indocyanine-green (ICG) accumulates in areas of permeable endothelium (i.e. peritumoral tissue) over >16 h (hence, imaging during the "Second-Window" rather than immediately after ICG infusion) via the enhanced-permeability-and-retention (EPR) effect [25–28].

Previously, we demonstrated a proof-of-concept using SWIG in detecting tumor specimens in 10 HGG patients, with higher sensitivity (86% vs 77%) compared to white-light alone. In this larger study, we further demonstrate the ability of SWIG to predict postoperative MRI findings while still in the operating room – thus providing a technique that may offer MRI-like imaging without the cumbersome and expensive requirements of true iMRI.

Materials and Methods

Study Population

All patients >18-years undergoing resection of central nervous system tumors were prospectively enrolled between October 2014 and October 2018 in an IRB-approved, registered trial. Exclusion criteria were pregnancy and allergy to contrast dye, iodide or shellfish. All patients gave informed consent for this study. For this retrospective analysis, data from all patients with pathology-proven, newly-diagnosed HGG were collected.

Preoperative Assessment

All patients underwent preoperative 1mm-slice MRI of the brain with intravenous gadolinium. MRI analysis and volumetric calculations were performed using GE PACS (General Electric Healthcare, Chicago, IL) and BrainLab (Brainlab, Munich, Germany) software.

Near-Infrared Contrast Agent

Before April 2018, patients were infused intravenously with a 5mg/kg dose of ICG ($C_{43}H_{47}N_2O_6S_2.Na$; Akorn Pharmaceuticals, Illinois, USA) approximately 24 h before surgery at an outpatient infusion center. As of April 2018, the ICG dose was decreased to 2.5mg/kg as part of a dose de-escalation study currently underway and as a cost-reducing measure [29].

Near-Infrared Imaging System

All cases were imaged using the FDA-approved VisionSense Iridium™ exoscope (VisionSense, Philadelphia, PA) with a NIR laser excitation source (805 nm) and camera (820–860nm), which has very high NIR sensitivity and dynamic range [30, 31]. Furthermore, the VisionSense allows white-light and NIR imaging to be overlaid in real-time, preserving background anatomic information.

Author Manuscript Author Manuscript Author Manuscript Author Manuscript

Study Procedure

Standard-of-care resections were performed as previously described [26, 27]. Upon craniectomy, room lights were dimmed and window shades were closed to eliminate stray infrared light. The sterile-draped NIR exoscope was positioned above the operative field. NIR signal was documented at this time (Dura-View). The dura was then opened and NIR signal was recorded (Cortex-View). For deep tumors, the presence of NIR signal was recorded again following corticectomy to reveal the tumor (Tumor-View). After resection of the gross tumor using white-light microscopy, both white-light and NIR imaging were used to examine the margins (Margin-View). Areas that seemed neoplastic under white-light were resected regardless of NIR fluorescence, although in-vivo NIR fluorescence presence/absence in those areas was recorded prior to resection. If there were areas that did not appear convincing for tumor under white-light but demonstrated NIR fluorescence, small biopsy specimens were taken. Due to the experimental nature of the SWIG protocol, resection was not guided by NIR imaging alone; thus, areas of residual NIR fluorescence were left unresected (other than small biopsies) if the surgeon would not have resected the area otherwise. All biopsy specimens were sent to pathology. One final NIR imaging was performed prior to surgical closure (Final-View). Postoperatively, patients underwent standard-of-care treatment under the Stupp protocol.[32]

Evaluation of Near-Infrared Signal

Videos of the tumor resection were recorded and analyzed postoperatively by three independent reviewers. The presence or absence of NIR signal, as well as the signal-to-background-ratio (SBR) was analyzed at all views. The SBR was calculated using ImageJ (National Institute of Health, Bethesda, MD) to measure the mean pixel intensity within the area of interest, divided by the mean pixel intensity in an area corresponding to normal brain parenchyma [31]. SBR greater than 2.0 was deemed significant, based on our prior intraoperative experiences.

Videos from the Margin-View and Final-View were particularly closely observed. Each Margin-View video was matched with the corresponding biopsy specimen in order to accurately calculate the test characteristics for NIR imaging. With Final-View imaging, if residual NIR fluorescence was noted in or around the surgical cavity, the anatomic location of the fluorescence was determined (i.e. anterior-cavity, posterior-cavity, deep-cavity, etc.) in order to compare this location to the location of any residual gadolinium enhancement seen on postoperative MRI. Due to neuronavigation's limitations in accounting for brain-shift and other changes, we did not rely on neuronavigation to evaluate the areas of residual NIR fluorescence.

Evaluation of Postoperative MRI

MRIs were performed the morning after surgery using either 1mm or 5mm-slices per hospital protocol. All MRIs were reviewed by neuroradiologists who were blinded to the NIR imaging results. Locations of residual gadolinium enhancement were reported on the radiology reports. BrainLab software was used by two blinded authors to perform manual volumetric analyses on any residual gadolinium-enhancing components. Patients with zero residual enhancements were considered to have complete-resection-of-enhancing-tumor

Author Manuscript Author Manuscript Author Manuscript Author Manuscript

(CRET) as suggested by the Response Assessment in Neuro-Oncology (RANO) Working Group [33]. Patients received regular follow-ups and serial MRI scans to track recurrence (new gadolinium enhancement) or progression of the tumor (>25% increase in perpendicular diameters of initial residual enhancement) as defined by the modified RANO criteria [34].

Clinical Data Collection

Clinical data on patients were retrospectively collected, with the most recent data collected on January 2019. Potential prognostic factors, such as age, gender, isocitrate-dehydrogenase (IDH) mutation status, tumor location, and preoperative tumor volume were collected. For calculation of Cox-hazard ratios, age and preoperative tumor volume were converted to a dichotomous variable (>/< 65 years of age and >/< 15cm^3 (median volume), respectively).

All patients in this study continued to receive care at our institution after surgical intervention. Overall-survival (OS) was calculated from the date of surgery until death or until January 2019 for those still alive. Progression-free-survival (PFS) was calculated from the date of surgery until recurrence/progression of the tumor as defined above, death in those that died without radiologic evidence of recurrence/progression, or until January 2019 for those still alive without recurrence/progression.

Statistical Analysis

Statistical analyses were performed using STATA 10™ (StataCorp LLC, Collegestation, TX). The Mann-Whitney test was used when comparing values. Two-by-two contingency tables were constructed to calculate the sensitivity/specificity/positive-predictive-value (PPV)/negative-predictive-value (NPV)/accuracy for the surgeon's impression and SWIG for neoplastic tissue. Kaplan-Meier curves of PFS and OS were constructed using STATA and Cox-hazard ratios were calculated for potential prognostic variables. A p-value cutoff of <0.05 was used to determine statistical significance and 95% confidence intervals (CI) were used.

Results

NIR visualization using SWIG provides strong tumor-to-brain contrast as ICG accumulates within the tumor and is rapidly cleared from normal brain parenchyma. We present three results to validate performance characteristics of SWIG as a diagnostic tool. First, fluorescence imaging results will be presented at the dura, cortex (prior to corticectomy) and at the direct tumor view. Next, we present information on margin specimen analysis comparing white-light to NIR for tumor detection. Finally, we present data showing that NIR imaging can predict both the presence and location of gadolinium enhancement on postoperative MRI with high accuracy.

Participants

Thirty-six patients with primary HGG (Grade IV) with no prior surgery/radiation were enrolled between October 2014 and October 2018 by two surgeons (SB, JYKL) (Table 1). Median preoperative tumor volume was 15.1cm^3 (range 1.5–115.8cm^3). The median interval between ICG infusion and intraoperative visualization was 22.2 h. Two patients had

Author Manuscript Author Manuscript Author Manuscript Author Manuscript

unforeseen events not attributable to the infusion that precluded surgery within the 24 h time window (53 and 120 h). All patients tolerated ICG infusions (28 patients at 5mg/kg; 8 patients at 2.5mg/kg) without major adverse events and no permanent surgical complications were identified.

Intraoperative Near-Infrared Visualization of Tumor

NIR imaging through intact dura was performed in 35 out of the 36 cases. The deepest tumor that was successfully visualized with NIR imaging was 13.3mm below the intact dura on preoperative MRI. Overall, 100% (14/14) of tumors reaching the cortex and 90% (27/30) of tumors ≤15mm below the cortex were visualized through the dura with NIR imaging. This is consistent with prior observations that NIR fluorescence, unlike visible light, can penetrate through dura and brain parenchyma up to approximately 1–1.5cm [25–27].

Furthermore, all 36 lesions demonstrated tumor-specific NIR fluorescence (SBR = 6.8 ± 2.2) when in direct sight of the NIR camera (Tumor-View). Patients who received 5mg/kg of ICG demonstrated stronger NIR fluorescence (SBR = 7.2 ± 2.2) than those that received 2.5mg/kg (5.2 ± 1.6, p-value = 0.0096); other factors did not significantly affect the NIR SBR.

These data confirm strong localization of ICG within tumor with excellent SBR that can be appreciated through the dura, through normal cortex, and upon direct inspection.

Near-Infrared Fluorescence Detection of Neoplastic Tissue

From the 36 patients, a total of 78 specimens were biopsied and labeled by the surgeon as consistent with tumor/not-tumor based on white-light visualization and yes/no for the presence of NIR fluorescence. On histopathology using H&E microscopic analysis, 69 specimens contained tumor cells. No additional markers of tumor presence, such as immunohistochemistry staining, Ki-67, or stem-cell traits, were used to determine the presence of tumor in the margin specimens. In all 78 specimens, white-light alone had 78% sensitivity, 100% specificity, 100% PPV, 38% NPV, and 81% accuracy. NIR, in contrast, had 97% sensitivity, 56% specificity, 94% PPV, 71% NPV, and 92% accuracy (Table 2).

Post-Resection Near-Infrared Imaging Correlation to Postoperative MRI

Upon resection of gross tumor and removal of margin samples, a final view of the operative cavity was performed with the NIR camera (Final-View) in 34 patients; in two patients, Final-View was not imaged due to technical reasons. Residual areas of NIR fluorescence were video-recorded after biopsies were completed; these images were then oriented in 3-dimensional space and compared to postoperative MRI performed within 24 h, which served as the gold-standard of determining the extent of resection. No further biopsies were performed during/after the Final-View, precluding histopathological correlates.

In 25 of the 34 patients, the Final-View NIR imaging demonstrated residual NIR fluorescence. In 23 of these 25 patients, postoperative MRI demonstrated residual neoplasm (0.3–37.3cm^3), and the location of the residual NIR fluorescence correlated with the location of the residual gadolinium enhancement (Fig. 1). Thus, Final-View NIR imaging was highly

Author Manuscript Author Manuscript Author Manuscript Author Manuscript

sensitive to residual gadolinium enhancement on postoperative MRI even to volumes as small as 0.3cm^3 in the appropriate anatomic location. In 2 of the 25 cases, nonspecific NIR fluorescence was visualized in patients with no residual enhancement on postoperative MRI (Fig. 2); this may have been due to ICG leaking out of the tumor during resection, as NIR signal was detected in previously clean regions. Thus, there were 23 true-positive signals and 2 false-positive signals with the Final-View NIR imaging.

In contrast, 9 of the 34 patients demonstrated no significant NIR fluorescence on Final-View. In 8 of these 9 patients, the immediate postoperative MRI demonstrated complete resection of enhancing tumor (CRET), defined as complete absence of residual gadolinium-enhancing volume (Fig. 3). In one patient, residual gadolinium enhancement measuring 5.4cm^3 was seen on postoperative MRI at 48mm below the cortex; this was attributed to potentially insufficient excitation of the deep tissue, discussed below. Thus, there were 8 true-negative and 1 false-negative readings with the Final-View NIR imaging.

In total, in these 34 patients, Final-View imaging resulted in 23 true-positive, 8 true-negative, 2 false-positive, and 1 false-negative signals for predicting the results of postoperative MRI, leading to 96% sensitivity (95% CI 79–100%), 80% specificity (44–97%), 92% PPV (77–98%), 89% NPV (53–98%), and 91% accuracy (76–98%). Furthermore, chi-squared analysis demonstrated a significant correlation (p-value < 0.0001) between residual NIR fluorescence and residual gadolinium enhancement.

Overall, in the 34 patients for whom volumetric analysis was available both before and after resection, the median tumor volume was 15.1cm^3 (range 1.5–115.8cm^3) preoperatively and 0.75cm^3 (range 0–37.3cm^3) postoperatively (Figure 4). CRET was achieved in 29.4% (10/34) of cases. This resection data was stratified according to the Final-View NIR imaging results (Table 3). Those with no residual NIR fluorescence on Final-View imaging were significantly more likely to demonstrate CRET on postoperative MRI (p-value<0.0001), have higher resection rates (p-value = 0.0011), and have smaller volumes of residual neoplasm (0.0027) than those with residual NIR fluorescence.

Finally, a stratified analysis of the resection data based on tumor location revealed no statistical difference in CRET rate (p-value=0.86) or Final-View NIR imaging accuracy (p-value = 0.44) between tumors in eloquent location (n=16) and non-eloquent location (n = 18).

Clinical Outcome

The median PFS for the patients in our study was 168 days (range 3–1237). There was no significant correlation between PFS and IDH status (p-value = 0.24), age over 65 years (p-value = 0.65), gender (p-value=0.34), or preoperative tumor volume (p-value = 0.55). Stratified analyses (Table 3) revealed a trend towards increased PFS in patients with CRET on postoperative MRI (p-value=0.12, Fig. 5a), but not in those with negative NIR fluorescence on Final-View (p-value=0.99, Fig. 5b).

The median OS for the patients was 484 days (range 3–1237). All 3 patients with IDH-mutated tumors remain alive at 152, 865, and 1104 days postoperatively, approaching

Author Manuscript Author Manuscript Author Manuscript Author Manuscript

statistical significance in increased OS (p-value = 0.08). There was no significant correlation between OS and age over 65 years (p-value 0.11), gender (p-value = 0.72), or preoperative tumor volume (p-value = 0.13). Stratified analyses (Table 3) revealed a trend towards statistical difference in OS for patients with CRET on postoperative MRI (p-value = 0.08, Fig. 5c), but not in those with negative NIR fluorescence on Final-View (p-value = 0.86, Fig. 5d).

Discussion

Complete surgical resection of high-grade gliomas cannot cure patients of disease; however, increasing the extent of resection (EOR) does contribute to improved overall survival and progression-free survival in patients with HGG [1, 2, 4, 5, 19]. The definition of EOR in HGG is based on gadolinium-enhancement, although the acceptance that HGG is an infiltrative disease with boundaries that likely extend beyond the gadolinium-enhancement [33, 34]. Thus, because current definitions of EOR depend on gadolinium enhancement and increased EOR has been shown to improve patient outcomes, it is imperative to provide the surgeon with real-time, intraoperative information that predicts gadolinium enhancement on MRI.

Optical methods that could predict gadolinium-enhancement on MRI are appealing and many groups have compared the utility of fluorescence-guided surgery (FGS) with 5-ALA against HGG resection using iMRI, with varying conclusions [35–37]. Here, we suggest that near-infrared imaging with SWIG can predict gadolinium enhancement on postoperative MRI.

In previous papers, our group has demonstrated that SWIG could be used to localize intracranial tumors (HGG, metastases, meningiomas) in real-time intraoperatively, suggesting its potentials as a FGS agent [25–27]. We hypothesize that ICG accumulates within tumors via the EPR effect, in which small molecules, such as ICG or gadolinium, accumulate in areas of high blood-brain-barrier permeability in the peritumoral tissue [38–41]. Further tumor-specificity may be conferred by active endocytosis of ICG by tumor cells, making it superior to fluorescein, which was not retained within intracellular compartments [42]. We previously demonstrated a long plateau period of visualization of ICG within tumors, thus providing immense flexibility in ability to use this technique for tumor surgery [43]. This prolonged dye accumulation within tumor cells thus differs from gadolinium, which is not known to significantly accumulate intracellularly [44].

Clinical Benefits of Near-Infrared Fluorescence-Guided Surgery

Currently, ICG remains the only FDA-approved near-infrared fluorophore for use in humans. Thus, SWIG leads the NIR FGS effort in terms of the number of patients that have received it. However, researchers of FGS are now intensely focusing on novel NIR agents that may exhibit more tumor specificity, through receptor targeting or metabolic specificity. Unlike 5-ALA, which is only amenable to FGS using visible-light excitation and emission, SWIG and these other novel agents fluoresce in the NIR region. Two major benefits of working in the NIR spectrum are the superior tissue penetration of NIR fluorescence and the ability to easily measure fluorescence intensity objectively. First, it is well known that photons

Author Manuscript Author Manuscript Author Manuscript Author Manuscript

in the NIR wavelength better penetrate tissue compared to visible spectrum photons due to reduced absorbance by endogenous fluorophores.[45] Thus, residual tumor that may be hidden behind normal tissue is much more likely to be detected using NIR fluorescence than with 5-ALA. Specifically, we demonstrated in this study that we could reliably detect tumors that were up to 15mm below the dura. Second, NIR fluorescence can be measured objectively. In this study and prior publications, we use an objective SBR measurement to quantify NIR fluorescence. In contrast, in the vast majority of literature investigating 5-ALA, the fluorescence is measured subjectively using either a +/− scale or at best, none/weak/strong red fluorescence. This leads to measurements that are inherently subjective and less reliable. This subjectivity is largely due to the fact that humans can readily see the red fluorescence, making a subjective scale more accessible. While a detailed comparison between the clinical utility of 5-ALA and NIR agents is not yet available, most researchers have turned their focus to NIR agents for FGS for these clinical advantages.

Clinical Applicability of Second-Window Indocyanine-Green

In our study of 78 biopsy specimens from 36 patients who received SWIG, NIR imaging was more sensitive and had a higher NPV and accuracy for diagnosing neoplastic tissue intraoperatively, compared to white-light alone. Overall, this suggests that the greatest benefit of NIR imaging is in detecting areas of residual neoplasm that may be missed on white-light imaging. In fact, while NIR imaging did miss 2 neoplastic specimens, it detected 13 more neoplastic specimens compared to white-light alone, and all specimens that were deemed neoplastic under white-light fluoresced under NIR imaging. Thus, when the goal of surgery is to leave no residual tumor (i.e. tumors in non-eloquent locations), NIR imaging with SWIG could help to minimize residual neoplasm and improve patient outcomes.

Furthermore, we hypothesized that NIR imaging could predict gadolinium enhancement postoperatively. Our data suggests that the post-resection Final-View NIR imaging predicts gadolinium enhancement on postoperative T1-weighted MRI with 96% sensitivity and 91% accuracy. In this study, our IRB-approved protocol did not allow the surgeon to change the extent of resection based on NIR imaging, and as such, residual areas of NIR were only correlated with MRI findings. Furthermore, with this small retrospective study, we were unable to assess the impacts of NIR imaging results on patient outcome (PFS and OS showed no statistical difference). Nonetheless, we demonstrate several advantages of NIR imaging with SWIG. First, NIR imaging can detect residual gadolinium enhancement as small as $0.3cm^3$ in the proper corresponding location. Second, lack of NIR fluorescence on Final-View imaging correctly predicted complete resection of enhancing tumor (CRET) in 89% of cases. The one false-negative case had residual neoplasm that was ~5cm deep, which we discuss below as a limitation. Third, the corollary is that the presence of residual NIR fluorescence on Final-View imaging correctly predicted residual enhancing tumor on postoperative MRI in 92% of cases. Indeed, patients with negative Final-View NIR imaging were significantly more likely to achieve CRET. As such, we believe that SWIG provides surgeons with an alternative to visualize gadolinium-enhancement in real-time in the operating room.

Author Manuscript Author Manuscript Author Manuscript Author Manuscript

Limitations

There are limitations to NIR imaging using SWIG. In one patient with no NIR fluorescence on Final-View imaging, postoperative MRI demonstrated a 5.4cm^3 residual neoplasm located 48mm deep in a narrow cavity. Most likely, the excitation laser could not reach the tissue to excite the ICG. Although this is a limitation of NIR imaging, the depth of penetration is significantly greater than visible light dyes, such as 5-ALA and fluorescein. For such deep cavities and margins, using NIR-capable endoscopes, which we have investigated in transsphenoidal endoscopic surgeries, may be of use. Second, because the mechanism of action of SWIG relies on passive diffusion and accumulation via the EPR effect, ICG can accumulate in non-neoplastic areas of blood-brain-barrier breakdown, such as inflammation and/or necrosis (unpublished data), lowering the specificity. Finally, the SWIG protocol requires patients to visit the outpatient suite the day prior to surgery if they are not already inpatients, which may be cumbersome for some patients and surgeons. In contrast, 5-ALA can be given the day of surgery, which facilitates its administration. A shorter, same-day “Second-Window” for SWIG will be investigated in the future.

Ultimately, this study was a retrospective study performed to test our hypothesis based on past observations. While we were not able to directly compare NIR imaging to iMRI, we believe this study provides compelling evidence to support SWIG as a proxy for gadolinium enhancement on postoperative MRI scans. Given that iMRI and neuronavigation, both of which relies on gadolinium enhancement, have demonstrated the ability to help surgeons achieve increased resection rates, SWIG is a promising technique that may improve surgical outcomes by providing real-time detection of gadolinium-enhancing tissues intraoperatively.

Conclusion

In this study, we demonstrate the potential benefits of Second-Window-ICG as a near-infrared fluorescent dye technique for surgical localization of high-grade-gliomas prior to dura opening and prior to corticectomy. In addition, SWIG can predict the presence/location of gadolinium enhancement on postoperative MRI. Future directions of study include comparisons to 5-ALA and iMRI. Oncologic surgery is currently at the cusp of rapid introduction of targeted, near-infrared fluorophores; although SWIG is not a targeted dye and instead relies on passive diffusion, EPR, and intracellular endocytosis, it nonetheless provides a valuable framework for analysis of near-infrared workflow during neurosurgery.

Acknowledgements

Funding: Supported in part by the National Institutes of Health R01 CA193556 (SS), and the Institute for Translational Medicine and Therapeutics of the Perelman School of Medicine at the University of Pennsylvania (JYKL). Research reported in this publication was also supported by the National Center for Advancing Translational Sciences of the National Institutes of Health under Award Number UL1TR000003 (JKYL). In addition, research reported in this publication was supported by the National Center for Advancing Translational Sciences of the National Institutes of Health under award number TL1TR001880 (SSC). The content is solely the responsibility of the authors and does not necessarily represent the official views of the NIH.

References

1. Lacroix M, Abi-Said D, Fourney DR, et al. (2001) A multivariate analysis of 416 patients with glioblastoma multiforme: prognosis, extent of resection, and survival. J Neurosurg 95:190–198.

Author Manuscript Author Manuscript Author Manuscript Author Manuscript

2. Sanai N, Polley M- Y, McDermott MW, et al. (2011) An extent of resection threshold for newly diagnosed glioblastomas. J Neurosurg 115:3–8. [PubMed: 21417701]

3. Stummer W, Kamp MA (2009) The importance of surgical resection in malignant glioma. Curr Opin Neurol 22:645–649. [PubMed: 19738467]

4. Sanai N, Berger MS (2011) Extent of resection influences outcomes for patients with gliomas. Rev Neurol 167:648–654. [PubMed: 21903234]

5. Sanai N, Berger MS (2008) Glioma extent of resection and its impact on patient outcome. Neurosurgery 62:753–764 [PubMed: 18496181]

6. Berkmann S, Schlaffer S, Nimsky C, et al. (2014) Intraoperative high-field MRI for transsphenoidal reoperations of nonfunctioning pituitary adenoma. J Neurosurg.

7. Kuo JS, Barkhoudarian G, Farrell CJ, et al. (2016) Congress of Neurological Surgeons Systematic Review and Evidence-Based Guideline on Surgical Techniques and Technologies for the Management of Patients With Nonfunctioning Pituitary Adenomas. Neurosurgery 79:E536–E538. [PubMed: 27635962]

8. Sheehan J, Lee C- C, Bodach M, et al. (2016) Congress of Neurological Surgeons Systematic Review and Evidence-Based Guideline for the Management of Patients With Residual or Recurrent Nonfunctioning Pituitary Adenomas. Neurosugery 79:539–540.

9. Rainer Wirtz WS, Albert FK, Schwaderer M, et al. (2016) The benefit of neuronavigation for neurosurgery analyzed by its impact on glioblastoma surgery. Neurol Res.

10. Sherman JH, Hoes K, Marcus J, et al. (2011) Neurosurgery for Brain Tumors: Update on Recent Technical Advances. Curr Neurol Neurosci Rep 11:313–319. 10.1007/s11910-011-0188-9 [PubMed: 21327735]

11. Mislow JMK, Golby AJ, Black PM (2009) Origins of intraoperative MRI. Neurosurg Clin N Am 20:137–46. [PubMed: 19555875]

12. Li P, Qian R, Niu C, Fu X (2017) Impact of intraoperative MRI-guided resection on resection and survival in patient with gliomas: a meta-analysis. Curr Med Res Opin 33:621–630. [PubMed: 28008781]

13. Napolitano M, Vaz G, Lawson TM, et al. (2014) Glioblastoma surgery with and without intraoperative MRI at 3.0T. Neurochirurgie 60:143–150. [PubMed: 24975207]

14. Kubben PL, Scholtes F, Schijns OEMG, et al. (2014) Intraoperative magnetic resonance imaging versus standard neuronavigation for the neurosurgical treatment of glioblastoma: A randomized controlled trial. Surg Neurol Int 5:70. [PubMed: 24991473]

15. Hatiboglu MA, Weinberg JS, Suki D, et al. (2009) Impact of Intraoperative High Field Magnetic Resonance Imaging Guidance on Glioma Surgery. Neurosurgery 64:1073–1081. [PubMed: 19487886]

16. Senft C, Bink A, Franz K, et al. (2011) Intraoperative MRI guidance and extent of resection in glioma surgery: A randomised, controlled trial. Lancet Oncol 10.1016/S1470-2045(11)70196-6

17. Kubben PL, ter Meulen KJ, Schijns OEMG, et al. (2011) Intraoperative MRI-guided resection of glioblastoma multiforme: A systematic review. Lancet Oncol 12:1062–1070. [PubMed: 21868286]

18. Stummer W, Stocker S, Wagner S, et al. (1998) Intraoperative detection of malignant gliomas by 5-aminolevulinic acid-induced porphyrin fluorescence. Neurosurgery 42:518–25; discussion 525–6 [PubMed: 9526986]

19. Stummer W, Pichlmeier U, Meinel T, et al. (2006) Fluorescence-guided surgery with 5-aminolevulinic acid for resection of malignant glioma: a randomised controlled multicentre phase III trial. 7:392–401

20. van Dam GM, Themelis G, Crane LMA, et al. (2011) Intraoperative tumor-specific fluorescence imaging in ovarian cancer by folate receptor-α targeting: first in-human results. Nat Med 17:1315–1319. [PubMed: 21926976]

21. Elliott JT, Marra K, Evans LT, et al. (2017) Simultaneous in vivo fluorescent markers for perfusion, protoporphyrin metabolism and EGFR expression for optically guided identification of orthotopic glioma HHS Public Access. Clin Cancer Res 23:2203–2212. [PubMed: 27799250]

22. Stummer W, Suero Molina E (2017) Fluorescence Imaging/Agents in Tumor Resection. Neurosurg Clin N Am 28:569–583. [PubMed: 28917285]

Author Manuscript Author Manuscript Author Manuscript Author Manuscript

23. Frangioni J V (2003) In vivo near-infrared fluorescence imaging. Curr Opin Chem Biol 7:626–34 [PubMed: 14580568]
24. Padalkar M V, Pleshko N (2015) Wavelength-dependent penetration depth of near infrared radiation into cartilage. Analyst 140:2093–100. [PubMed: 25630381]
25. Lee JYK, Pierce JT, Thawani JP, et al. (2017) Near-infrared fluorescent image-guided surgery for intracranial meningioma. J Neurosurg 1–11.
26. Lee JYK, Pierce JT, Zeh R, et al. (2017) Intraoperative Near-Infrared Optical Contrast Can Localize Brain Metastases. World Neurosurg 106:120–130. [PubMed: 28669877]
27. Lee JYK, Thawani JP, Pierce J, et al. (2016) Intraoperative Near-Infrared Optical Imaging Can Localize Gadolinium-Enhancing Gliomas During Surgery. Neurosurgery 79:856–871. [PubMed: 27741220]
28. Cho SS, Salinas R, Lee JYK (2019) Indocyanine-Green for Fluorescence-Guided Surgery of Brain Tumors: Evidence, Techniques, and Practical Experience. Front Surg 6:11. [PubMed: 30915339]
29. Newton AD, Predina JD, Corbett CJ, et al. (2019) Optimization of Second Window Indocyanine Green for Intraoperative Near-Infrared Imaging of Thoracic Malignancy. J Am Coll Surg 228:188–197. [PubMed: 30471345]
30. Dsouza A V, Lin H, Henderson ER, et al. (2016) Review of fluorescence guided surgery systems: identification of key performance capabilities beyond indocyanine green imaging. J Biomed Opt 1:.
31. Cho SS, Zeh R, Pierce JT, et al. (2018) Comparison of Near-Infrared Imaging Camera Systems for Intracranial Tumor Detection. Mol Imaging Biol 20:213–220. [PubMed: 28741043]
32. Stupp R, Mason WP, van den Bent MJ, et al. (2005) Radiotherapy plus Concomitant and Adjuvant Temozolomide for Glioblastoma. N Engl J Med 352:987–996. [PubMed: 15758009]
33. Vogelbaum MA, Jost S, Aghi MK, et al. (2012) Application of novel response/progression measures for surgically delivered therapies for gliomas: Response Assessment in Neuro-Oncology (RANO) Working Group. Neurosurgery 70:234–43; discussion 243–4. [PubMed: 21593697]
34. Ellingson BM, Wen PY, Cloughesy TF (2017) Modified Criteria for Radiographic Response Assessment in Glioblastoma Clinical Trials. Neurotherapeutics 14:307–320. [PubMed: 28108885]
35. Coburger J, Wirtz CR (2019) Fluorescence guided surgery by 5-ALA and intraoperative MRI in high grade glioma: a systematic review. J Neurooncol 141:533–546. [PubMed: 30488293]
36. Roder C, Bisdas S, Ebner FH, et al. (2014) Maximizing the extent of resection and survival benefit of patients in glioblastoma surgery: High-field iMRI versus conventional and 5-ALA-assisted surgery. Eur J Surg Oncol 40:297–304. [PubMed: 24411704]
37. Dg B, Bryant A, Vale L, et al. (2018) Intraoperative imaging technology to maximise extent of resection for glioma (Review) Cochrane Database of Systematic Reviews. 10.1002/14651858.CD012788.pub2.
38. Jiang JX, Keating JJ, De Jesus EM, et al. (2015) Optimization of the enhanced permeability and retention effect for near-infrared imaging of solid tumors with indocyanine green. Am J Nucl Med Mol Imaging 5:390–400 [PubMed: 26269776]
39. Madajewski B, Judy BF, Mouchli A, et al. (2012) Intraoperative Near-Infrared Imaging of Surgical Wounds after Tumor Resections Can Detect Residual Disease. Clin Cancer Res 18:5741–5751. [PubMed: 22932668]
40. Torchilin V (2011) Tumor delivery of macromolecular drugs based on the EPR effect. Adv Drug Deliv Rev 63:131–135. [PubMed: 20304019]
41. Weinmann H, Brasch R, Press W, Wesbey G (1984) Characteristics of gadolinium-DTPA complex: a potential NMR contrast agent. Am J Roentgenol 142:619–624. [PubMed: 6607655]
42. Onda N, Kimura M, Yoshida T, Shibutani M (2016) Preferential tumor cellular uptake and retention of indocyanine green for in vivo tumor imaging. Int J Cancer 139:673–682. [PubMed: 27006261]
43. Zeh R, Sheikh S, Xia L, et al. (2017) The second window ICG technique demonstrates a broad plateau period for near infrared fluorescence tumor contrast in glioblastoma. PLoS One 12:e0182034.
44. Aime S, Caravan P (2009) Biodistribution of gadolinium-based contrast agents, including gadolinium deposition. J Magn Reson Imaging 30:1259–67. [PubMed: 19938038]

Author Manuscript Author Manuscript Author Manuscript Author Manuscript

45. Teraphongphom N, Kong CS, Warram JM, Rosenthal EL (2017) Specimen mapping in head and neck cancer using fluorescence imaging. Laryngoscope Investig Otolaryngol 2:447–452.

Author Manuscript Author Manuscript Author Manuscript Author Manuscript

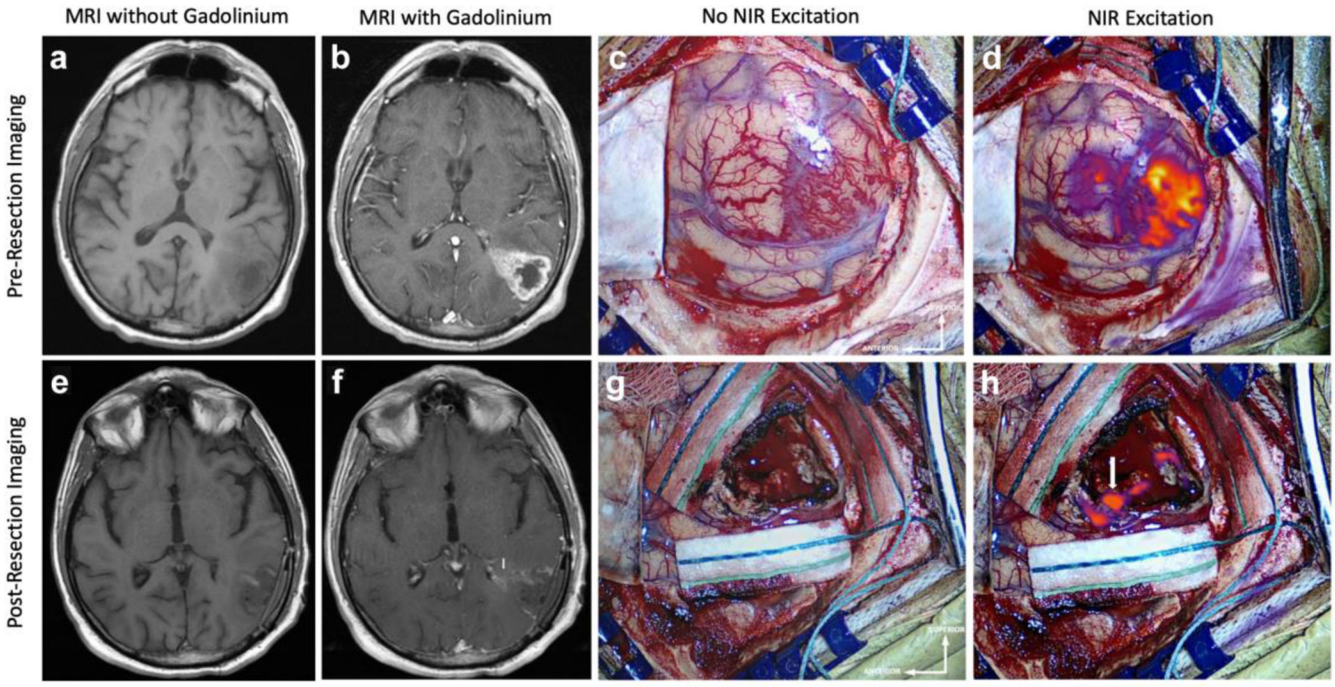

Figure 1:

NIR Imaging Correctly Predicts Residual Enhancing Tumor on Postoperative MRI Preoperative MRI, **a** without and **b** with gadolinium contrast, demonstrates a 20.3cm^3 contrast-enhancing lesion suggestive of HGG that extends to the cortex. **c** White-light imaging of the cortex after durotomy shows an area of hypervascularity suggestive of neoplasm. **d** NIR imaging after durotomy visualizes the superficial aspect of the tumor with a NIR SBR of 5.0. This NIR signal corresponds to the contrast-enhancement seen in **b**. Postoperative MRI, **e** without and **f** with gadolinium contrast, demonstrates subtotal resection of the contrast-enhancing tissue with a 0.9cm^3 area of residual enhancement in the deep portion of the resection cavity near the atrium of the left lateral ventricle (white arrow). **g** White-light imaging of the surgical cavity after resection does not reveal any areas of residual neoplasm. **h** Post-resection Final-View NIR imaging demonstrates removal of most areas of fluorescence. There remains residual NIR signal (SBR = 9.5) in the posterior portion deep in the resection cavity adjacent to the atrium of the left lateral ventricle (white arrow), consistent with the postoperative MRI finding.

Author Manuscript Author Manuscript Author Manuscript Author Manuscript

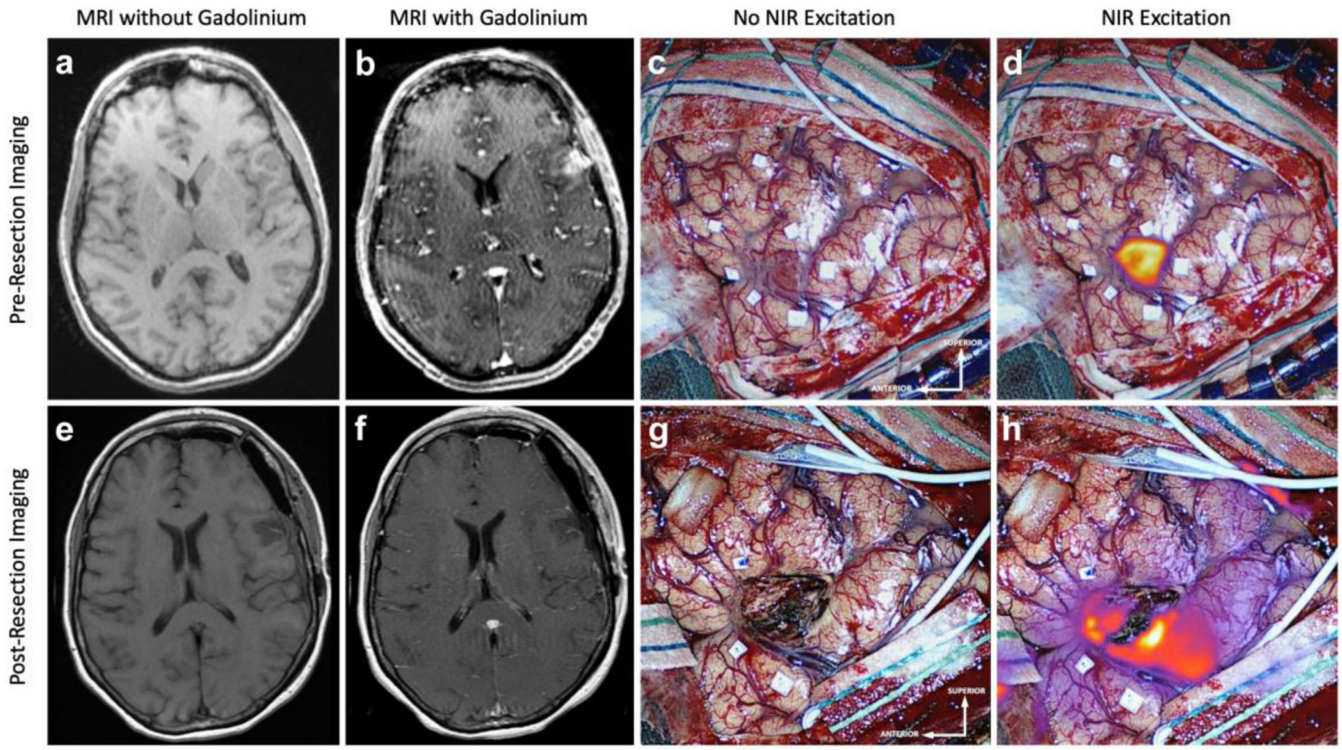

Figure 2:

False Positive NIR Signal on Final-View NIR Imaging: Preoperative MRI **a** without and **b** with gadolinium contrast, demonstrates a 1.5cm^3 contrast-enhancing lesion that extends to the cortex. **c** White-light imaging after durotomy reveals an area of discoloring consistent with neoplasm. **d** NIR imaging after durotomy visualizes this superficial tumor with a NIR SBR of 7.5. This NIR signal corresponds to the contrast-enhancement seen in **b**. Postoperative MRI, **e** without and **f** with gadolinium contrast, demonstrates CRET with no areas of residual enhancement. **g** White-light imaging of the surgical cavity after resection does not reveal any areas of residual neoplasm. **h** Post-resection Final-View NIR imaging demonstrates areas of non-specific NIR signal surrounding the surgical cavity. This was not seen in **c**, suggesting that the ICG may have leaked out of the tumor into the surrounding area during the resection.

Author Manuscript Author Manuscript Author Manuscript Author Manuscript

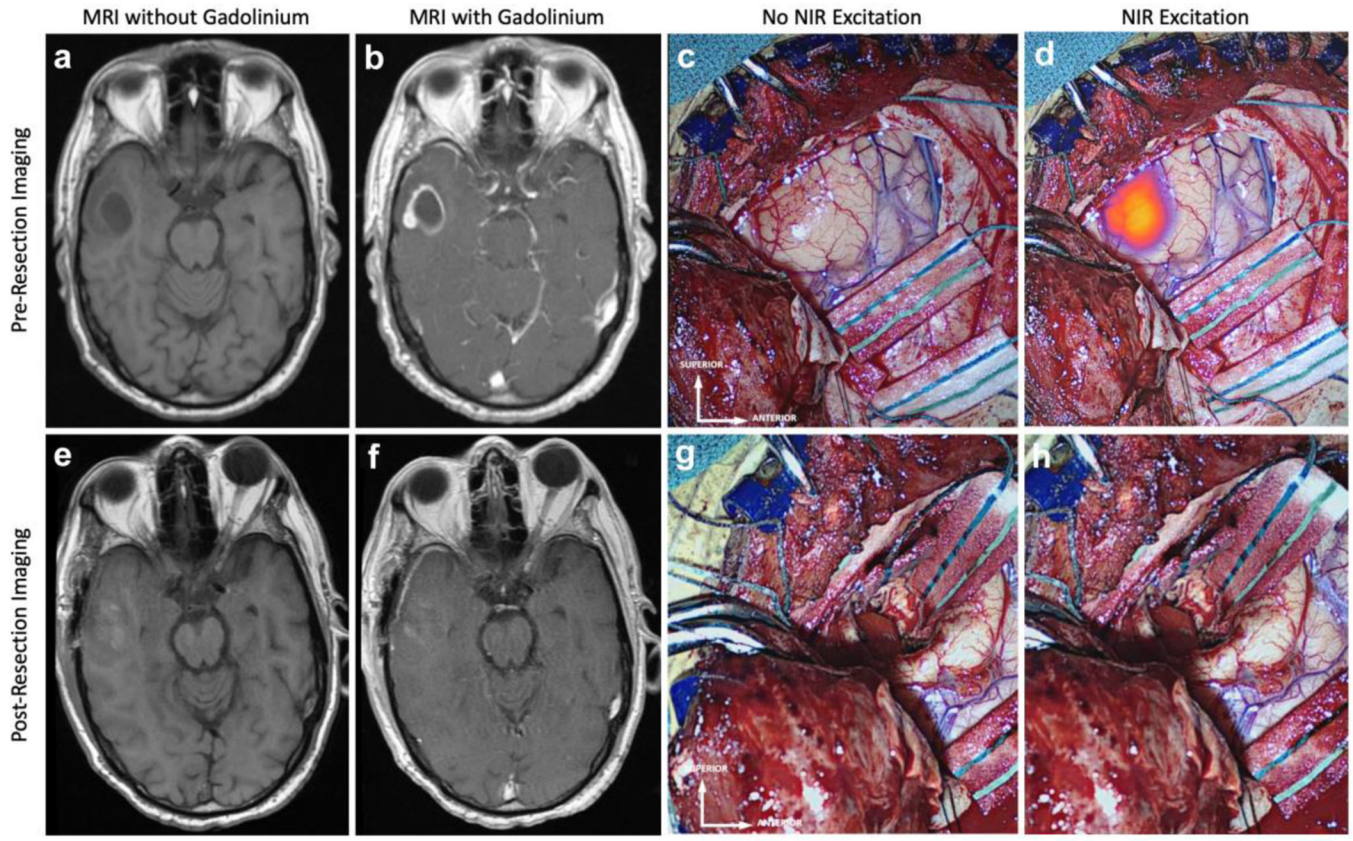

Figure 3:

Lack of NIR fluorescence on final-view NIR imaging correctly predicts complete resection of enhancing tumor on postoperative MRI: Preoperative MRI, **a** without and **b** with gadolinium contrast, demonstrates a 11.2cm^3 contrast-enhancing lesion 9mm below the cortex. **c** White-light imaging upon exposing the tumor reveals an area of hypervascularity suggestive of potential neoplasm. **d** NIR imaging after exposing the tumor visualizes this deep tumor with a NIR SBR of 7.8. This NIR signal corresponds to the contrast-enhancement seen in **b**. Postoperative MRI, **e** without and **f** with gadolinium contrast, demonstrates CRET with no area of residual enhancement. **g** White-light imaging of the surgical cavity after resection does not reveal any areas of residual neoplasm. **h** Post-resection Final-View NIR imaging demonstrates no areas of significant residual NIR fluorescence in the surgical cavity.

Author Manuscript Author Manuscript Author Manuscript Author Manuscript

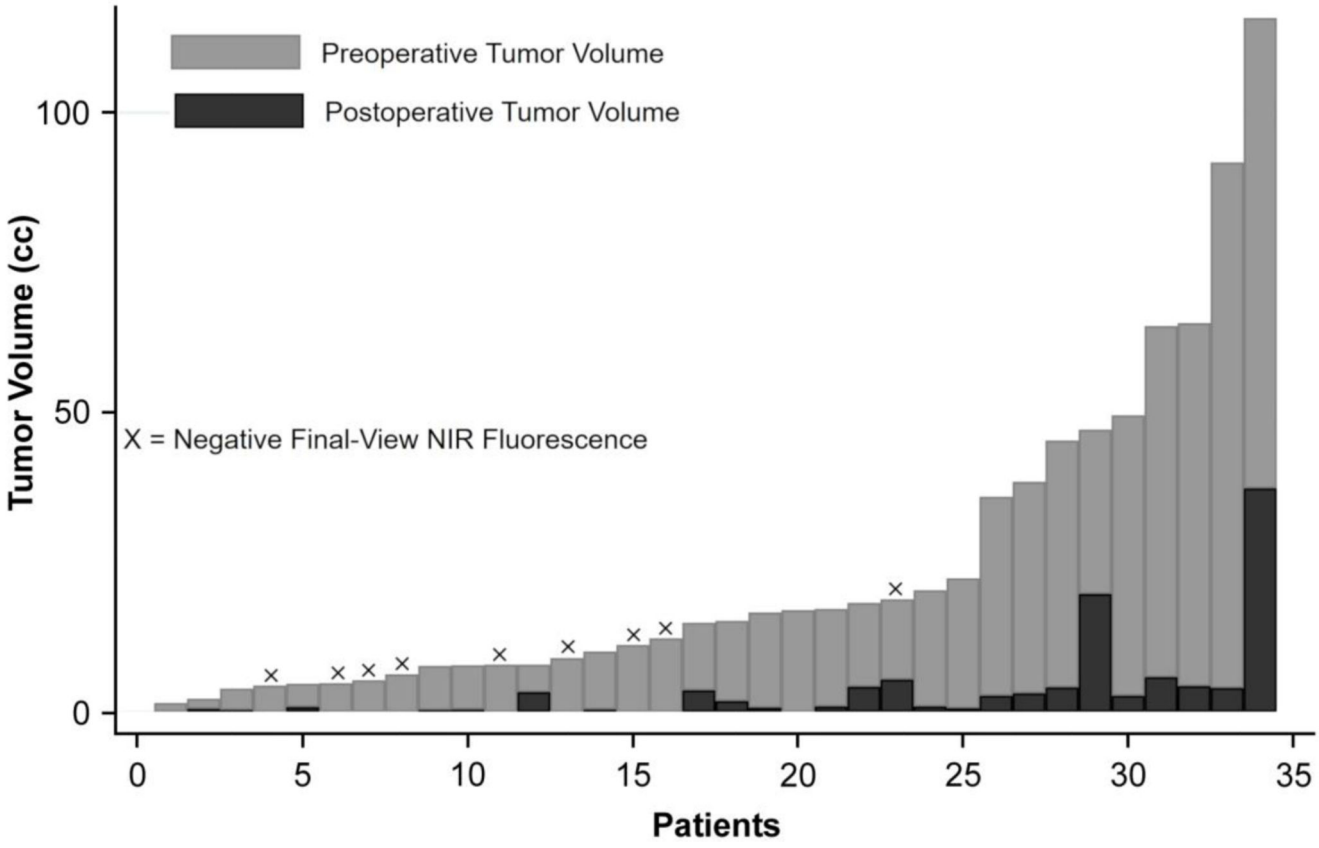

Figure 4:

Summary of preoperative and postoperative tumor volumes: In 34 patients in whom volumetric analysis was available, the median preoperative tumor volume (light gray bars) was 15.1cm^3 with a range of 1.5–115.8cm^3, while the median postoperative tumor volume (black bars) was 0.75cm^3 with a range of 0–37.3cm^3. The median resection rate was 94.8%. The 9 patients with no residual NIR signal on Final-View imaging are marked with an X. With the exception of 1 patient, all patients with negative Final-View NIR fluorescence demonstrated complete resection of enhancing components on postoperative MRI.

Author Manuscript Author Manuscript Author Manuscript Author Manuscript

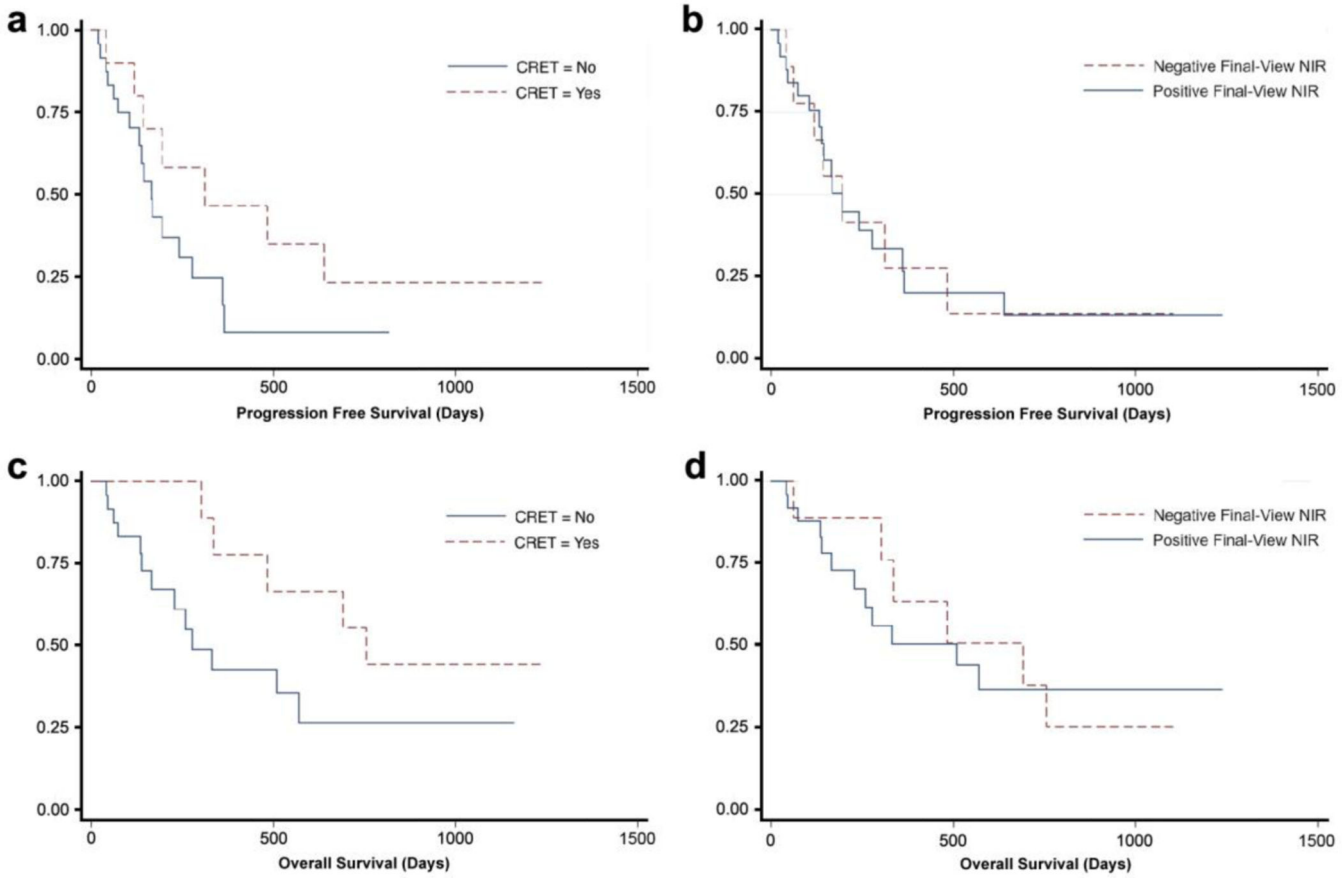

Figure 5:

Kaplan-Meier survival analysis: Subgroup analysis of PFS and OS based on postoperative MRI and Final-View NIR imaging results. **a** Patients with complete resection of enhancing tumor (CRET; $0cm^3$ of residual contrast enhancement) on postoperative MRI had a median PFS of 312 days, while those without CRET had a median PFS of 165 days. The difference in PFS was large, but not statistically significant (p-value = 0.12), likely due to small sample size. **b** There was no difference in PFS (195 days) between patients with no residual NIR fluorescence on Final-View imaging and those with residual NIR fluorescence (p-value = 0.99). **c** Patients with CRET on postoperative MRI had a median OS of 755 days, while those without CRET had a median OS of 278 days. The difference in OS was large, but not statistically significant (p-value = 0.08). **d** Patients with no residual NIR fluorescence on Final-View imaging had a median OS of 692 days, while those with residual NIR fluorescence had a median OS of 510 days. The difference in OS was large, but not statistically significant (p-value = 0.86)

Author Manuscript Author Manuscript Author Manuscript Author Manuscript

Table 1:

Demographic Data

Demographic Factor	Value
Patients (n)	36
Age (mean±SE)	65.3±2.3 (range 22–88)
Males (n)	20
Grade IV (n)	35
Grade III (n)	1
IDH Mutation (n, %)	3, 8.3%
Median preoperative tumor volume	15.1cm^3 (range 1.5–115.8cm^3)
Median postoperative tumor volume	0.75cm^3 (range 0–37.3cm^3)
Tumor depth (mean±SE, mm)	6.6±1.2 (range 0–27.9)
Tumor in eloquent location (n, %)	17, 47.2%
BMI (mean±SE)	27.1±0.57 (range 18.6–33.7)
Time from ICG infusion to imaging (mean±SE, hours)	25.9±2.9 (range 17.6–120)

Author Manuscript

Author Manuscript

Author Manuscript

Author Manuscript

Table 2

WL for all specimens

		White Light				Sensitivity	Specificity	PPV	NPV	Accuracy
		Yes	No		Point Estimate	78%	100%	100%	38%	81%
Tumor on pathology	Yes	54	15							
	No	0	9		95% CI	67–87%	NA	NA	28–48%	70–89%
		Total N	78							

NIR for all specimens

		NIR				Sensitivity	Specificity	PPV	NPV	Accuracy
		Yes	No		Point Estimate	97%	56%	94%	71%	92%
Tumor on pathology	Yes	67	2							
	No	4	5		95% CI	90–100%	21–86%	89–97%	36–92%	84–97%
		Total N	78							

Author Manuscript

Author Manuscript

Author Manuscript

Author Manuscript

Table 3:

Clinical Outcome Data Stratified by Final-View NIR Imaging

	Final-View NIR Imaging Negative for Residual Fluorescence	**Final-View NIR Imaging Positive for Residual Fluorescence**	**P-value**
N	9	25	NA
Age	57±21	68±9.2	0.40
Gender (% Male)	66.7	48	0.34
Median Preoperative Tumor Volume	7.9cm^3	17.2cm^3	0.035
Median Postoperative Tumor Volume	0cm^3	1.8cm^3	0.0027
CRET Rate	77.8%	8%	<0.0001
Mean Resection Rate	95.3±10.1%	87.9±12.1%	0.0099
Median PFS Length	195 days	195 days	0.99
PFS Rate at 6 months	55.6%	56.0%	0.98
PFS Rate at 12 months	22.2%	16.0%	0.67
Median OS Length	692 days	510 days	0.86
OS Rate at 6 months	77.8%	56.0%	0.25
OS Rate at 12 months	55.6%	32.0%	0.21